ACS Catalysis

Letter

pubs.acs.org/acscatalysis

Diamine-Alkalized Reduced Graphene Oxide: Immobilization of Sub-2 nm Palladium Nanoparticles and Optimization of Catalytic Activity for Dehydrogenation of Formic Acid

Fu-Zhan Song,[†,‡,§] Qi-Long Zhu,[†,§] Nobuko Tsumori,[†,#] and Qiang Xu*[,†,‡]

[†]National Institute of Advanced Industrial Science and Technology (AIST), Ikeda, Osaka 563-8577, Japan

[‡]Graduate School of Engineering, Kobe University, Nada Ku, Kobe, Hyogo 657-8501, Japan

[#]Toyama National College of Technology, 13, Hongo-machi, Toyama 939-8630, Japan

Supporting Information

ABSTRACT: An efficient strategy to downsize metal nanoparticles (NPs) and provide basic sites located nearby for optimizing the catalytic performance of reduced graphene oxide (rGO)-supported metal catalysts has been explored, for the first time, by potent alkalization of rGO with diamine. By virtue of the coordination effects between the metal ions and the amine groups ligated to rGO, monodispersed Pd nanoparticles (diameter ≤1.5 nm) can be facilely anchored on the diamine-alkalized rGO by a simple reduction approach. The turnover frequency (TOF) for heterogeneously catalyzed decomposition of formic acid reaches 3810 h^{-1} at 323 K, the highest value ever reported under ambient conditions compared with the other heterogeneous catalysts.

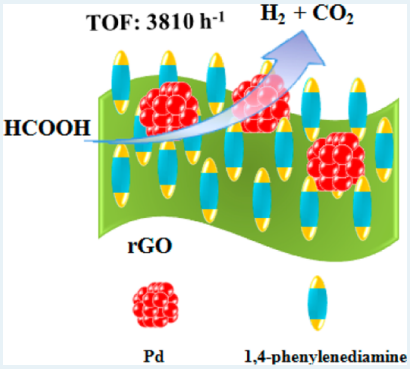

KEYWORDS: *dehydrogenation, formic acid, heterogeneous catalysis, nanoparticles, alkalized reduced graphene oxide*

Supported metal nanoparticles (NPs), as a class of very promising nanocatalysts, have received great interest. Nevertheless, the syntheses of well-dispersed ultrafine metal NPs remain a great challenge. The structure and property of support materials are crucial for controlling the growth of metal NPs and thus improving the catalytic performance.[1] Reduced graphene oxide (rGO) consisting of chemically converted monolayer carbon atoms has emerged as one of the most promising supports for metal NPs because the unique advantage of hydrophilicity and large specific surface area of its precursor, graphene oxide (GO), makes it possible to anchor metal NPs in the solution-based controlled reduction.[2] However, because of its two-dimensional basal plane structure and the negligible interactions between GO and metals, it is still a major obstacle to obtain monodispersed metal particles with very small sizes on GO, where it is difficult to perfectly overcome the aggregation of NPs.[3] Rational modification of the GO surfaces with electron-rich functional groups would facilitate the dispersion of the metal precursors on the support and control the size during the growth of metal NPs. Moreover, such modification may also provide an opportunity to tailor the electronic properties and alkalinity/acidity of GO, and thus optimize the catalytic performance of the resultant catalysts. Nevertheless, a well-defined and controllable surface modification strategy of pristine GO is still lacking.

Hydrogen is considered a promising candidate for satisfying the increasing demand for the sustainable and clean energy supply. Formic acid (FA) has attracted tremendous research interest for hydrogen storage.[4] Recently, selective and efficient decomposition of FA has been achieved with homogeneous organometallic catalysts.[5] Compared with homogeneous catalysts, in general, heterogeneous catalysts are easily separated, controlled and recycled.[6] For practical application, the development of heterogeneous catalysts with high performance for hydrogen generation from FA is urgently desired. Herein, for the first time, we report the immobilization of ultrafine Pd NPs on diamine-alkalized reduced graphene oxide, PDA-rGO (PDA = 1,4-phenylenediamine), which exhibits the highest TOF value (3810 h^{-1}, 323 K) for FA decomposition to H_2, and illustrate that the alkaline diamine on reduced graphene oxide (rGO) benefits dispersion of ultrafine Pd NPs and facilitates the decomposition of FA via the amine-assisted formate pathway.

The immobilization of Pd NPs to PDA-rGO is illustrated in Scheme 1 (see the Supporting Information for details). Addition of PDA into the aqueous solution of GO and stirring for 48 h resulted in the formation of a black precipitation (PDA-GO). The resultant PDA-GO precipitation was separated by centrifugation, washed with water, and subsequently dispersed in water, followed by addition of an aqueous solution of K_2PdCl_4. Finally, addition of $NaBH_4$ to the suspension and

Received: July 7, 2015
Revised: July 29, 2015
Published: July 30, 2015

DOI: 10.1021/acscatal.5b01411
ACS Catal. 2015, 5, 5141−5144

Scheme 1. Schematic Illustration for Pd/PDA-rGO Nanocatalyst Preparation

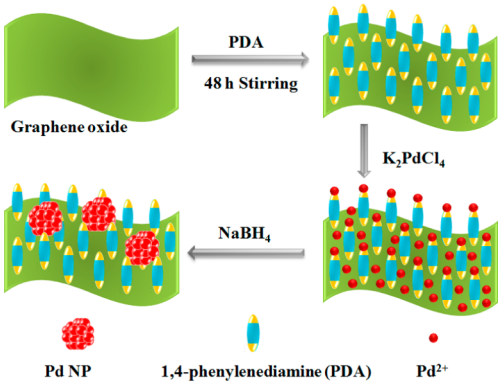

stirring for 45 min at room temperature resulted in the formation of ultrafine Pd NPs on the diamine-alkalized rGO, giving the Pd/PDA-rGO catalyst. For comparison, Pd/rGO was also synthesized using GO instead of PDA-GO.

Infrared spectroscopic (IR) measurements of PDA-GO and Pd/PDA-rGO reveal that most of the absorption bands from GO remain, except for the disappearance of the bands assigned to the C═O and epoxy C−O (Figure S4), and new bands are observed at 1158, 1623, and 3430 cm^{-1} due to the antisymmetric C−N stretching vibration, scissoring in-plane bending mode of $-NH_2$ groups, and the N−H stretching vibration, respectively, indicating the anchoring of amine groups on GO.[7] Raman spectroscopic measurements of GO and PDA-GO (Figure S5) show no changes in the peaks at 1600 (G band) and 1350 cm^{-1} (D band), confirming the retention of carbon framework with the addition of PDA.[8] The characteristic X-ray diffraction (XRD) for GO (2θ = 10.6°) is not observed for PDA-GO, suggesting disordered restacking of the PDA-GO layers (Figure S3). The diffractions at 39.8 (111) and 45.9° (200) for Pd (JCPDS: 46-1043)[2a] are observed for Pd/rGO but not for Pd/PDA-rGO, indicating the formation of very small Pd NPs on the diamine-functionalized rGO (Figure S3). The X-ray photoelectron spectroscopic (XPS) investigation further confirms the anchoring of amine groups to rGO, of which the signal is observed at 399.2 eV at the N 1s level. For Pd/rGO and Pd/PDA-rGO, the same binding energies (BEs) for Pd are observed at 335.6 and 340.9 eV, corresponding to Pd^0, at the Pd $3d_{5/2}$ and Pd $3d_{3/2}$ levels, respectively (Figures S7, S8). The corresponding energy dispersive X-ray (EDX) pattern confirms the existence of Pd (Figure 1d).

The morphologies of PDA-GO, Pd/rGO, and Pd/PDA-rGO are characterized by scanning electron microscopy (SEM). In all the samples, the continuous silk wave-like morphology is observed as a result of the interactions between graphene layers (Figure S9).[9] The transmission electron microscopy (TEM) and high-angle annular dark-field scanning TEM (HAADF-STEM) images of Pd/PDA-rGO show that discrete Pd NPs are homogeneously dispersed on rGO with an average size of 1.5 nm, ranging from 1.0 to 2.0 nm (Figures 1a−c and S11a). In contrast, when Pd NPs are directly supported on rGO, the NPs are severely aggregated with a much larger average particle size (10 nm) (Figures S10, S11b). The diamine groups not only highly disperse the GO against ordered restacking, but also provide coordinating groups to combine with Pd^{2+} ions,

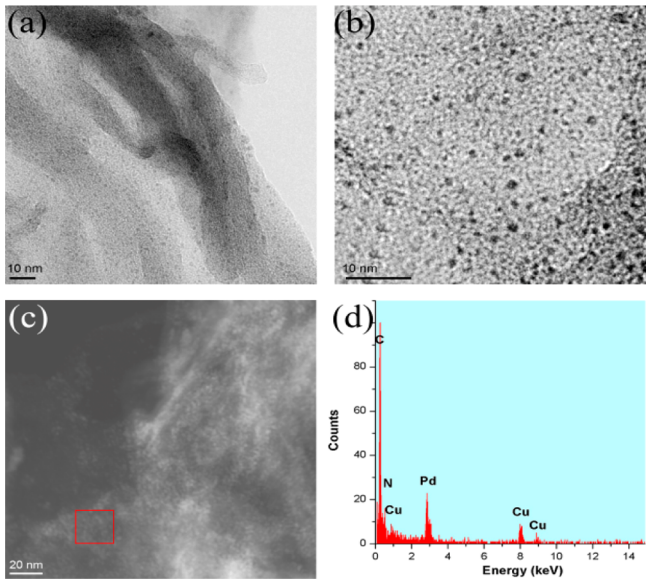

Figure 1. (a,b) TEM and (c) HAADF-STEM images of Pd/PDA-rGO, and (d) EDX pattern of the selected area in part c. The copper signals originate from the TEM grid.

resulting in rich and uniform nuclei and a controlled growth process of Pd on rGO.

Figure 2a shows the volume of the generated gas (CO_2 + H_2) versus time for the dehydrogenation of FA over Pd/PDA-rGO,

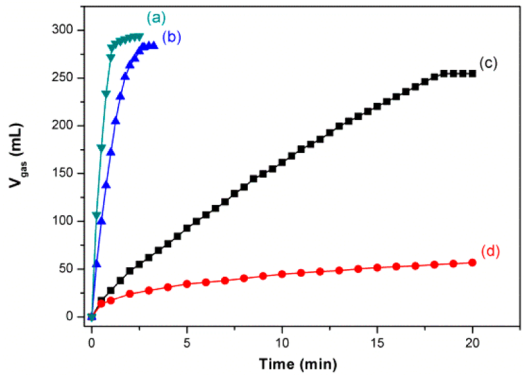

Figure 2. Volume of the generated gas (CO_2 + H_2) versus time for the dehydrogenation of (a) FA/SF (1:1) at 323 K and (b,c) pure FA at 323 and 298 K, respectively, over Pd/PDA-rGO and (d) the dehydrogenation of FA/SF (1:1) at 323 K over Pd/rGO (n_{Pd}/n_{FA} = 0.015).

which exhibits complete and selective decomposition of FA with an exceedingly fast kinetics. Within 1.05 min, 282 mL of gas can be generated from the FA/sodium formate (SF) system at 323 K (n_{Pd}/n_{FA} = 0.015, FA/SF = 1:1) (Figure 2a). The generated gas is identified by gas chromatography (GC) to be CO_2 and H_2, and no CO is detected at the level of detection limit (Figures S12, S13). It is noteworthy that the Pd/PDA-rGO gave an exceptional turnover frequency (TOF) of 3810 h^{-1}, the highest value ever reported for heterogeneously catalyzed FA decomposition, comparable to the most active homogeneous catalysts (Table S1). Even without any additive, the decomposition of pure FA can be completed in 2.67 and 18.5 min (n_{Pd}/n_{FA} = 0.015), corresponding to TOF values as

DOI: 10.1021/acscatal.5b01411
ACS Catal. 2015, 5, 5141−5144

high as 1500 and 216 h^{-1}, at 323 and 298 K, respectively (Figure 2b,c).

The gas generation rate over Pd/PDA-rGO catalyst greatly depends on the reaction temperature. The catalytic reactions are completed in 5.5, 4.17, 2.08, and 1.05 min at 298, 303, 313, and 323 K (n_{Pd}/n_{FA} = 0.015, FA/SF = 1:1) (Figure S14a), respectively, corresponding to TOF values of 727, 959, 1923, and 3810 h^{-1} (Figure S14b). The Arrhenius plot fitted on the basis of the TOF values for the decomposition of FA at different reaction temperatures gives an activation energy (E_a) of 54.3 kJ mol^{-1}. In addition, it is noteworthy that the molar ratio of FA to SF has an obvious effect on the performance of the synthesized Pd/PDA-rGO catalyst. With the increase in the molar percentage of SF in aqueous FA-SF solution, the catalytic activity increases initially and then decreases, with the best performance at a molar ratio of 1:1 (Figure S15).

We further examine briefly the stability of Pd/PDA-rGO catalyst by adding aliquots of FA (0.23 mL, 6.0 mmol) into the reactor after the reaction completion of the last run. No significant loss in activity and selectivity is observed over 5 cycles (Figure S16). TEM and XRD measurements of the recovered catalyst show no obvious change in the Pd particle size (Figures S17, S18), indicating that the Pd/PDA-rGO catalyst has high durability and stability under the current FA dehydrogenation conditions.

In contrast to the excellent catalytic performance of Pd/PDA-rGO, the Pd/rGO catalyst shows a very low activity for the decomposition of FA under the same conditions, over which only 52 mL of gas is released in 20 min (Figure 2d) (n_{Pd}/n_{FA} = 0.015, 323 K). It is well-known that the catalytic activity generally increases with a decrease in the metal NP size because smaller particles possess higher surface areas available for reactants. Reasonably, the decrease in the particle size of Pd NPs supported by PDA-rGO should be one of the most important factors that are responsible for the drastic enhancement in the catalytic activity. On the other hand, the alkalization of GO with diamine plays another important role in promoting the catalytic performance. To determine the effect of the amount of immobilized PDA on the catalytic activity, the GO supports with various mass ratios of PDA/GO have been synthesized for depositing Pd NPs (Figure S19, Table S2). With an increase in the mass ratio of PDA/GO to 5.4:1, the TOF value initially increases, but after reaching a maximum value of 3810 h^{-1}, a further increase in the amount of PDA shows a negative effect on the dehydrogenation of FA.

As illustrated in Scheme 2, the alkaline $-NH_2$ group, as a proton scavenger, benefits the antisymmetric cleavage of the O−H bond in the FA molecule, resulting in the formation of an intermediate palladium formate complex along with a $-[H_2NH]^+$ group during the initial step of the reaction. Subsequently, the palladium formate species could undergo β-hydride elimination to produce CO_2 and a palladium hydride species. The final hydrogen desorption step is combined with th $-[H_2NH]^+$ group and a palladium hydride species, which is irreversible and also kinetically relevant, highlighting the feasibility of renewable FA as a convenient in situ hydrogen source instead of molecular H_2 for sustainable and green organic synthesis.[10]

To demonstrate the universality of this synthetic strategy for introducing alkalinity to GO and supporting ultrafine metal NPs, different amine-rGO systems, including PDA-rGO (PDA = 1,4-phenylenediamine), AMA-rGO (AMA = 4-(aminomethyl)aniline), DAH-rGO (DAH = 1,6-diaminohexane), DMPDA-rGO (DMPDA = *N*,*N*-dimethyl-1,4-phenylenediamine) and A-rGO (A = aniline), have been prepared and subsequently used to immobilize Pd NPs. Figure 3 shows the catalytic performance of Pd NPs immobilized by these amine-alkalized rGO supports. Compared with Pd/rGO, all the catalysts exhibit exceedingly enhanced catalytic activities for hydrogen generation from FA; however, only a moderate enhancement is found for Pd/A-rGO, which may be due to the fact that in aniline, a monoamine molecule, the only $-NH_2$ group is covalently bound to rGO and thereby leads to a lack of the interactions with Pd, further indicating the unique role of the diamines in this system.

Scheme 2. Possible Reaction Pathway of Amine-Associated Decomposition of FA over Pd/PDA-rGO

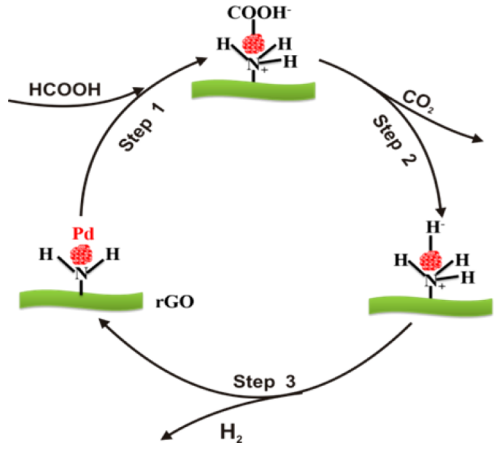

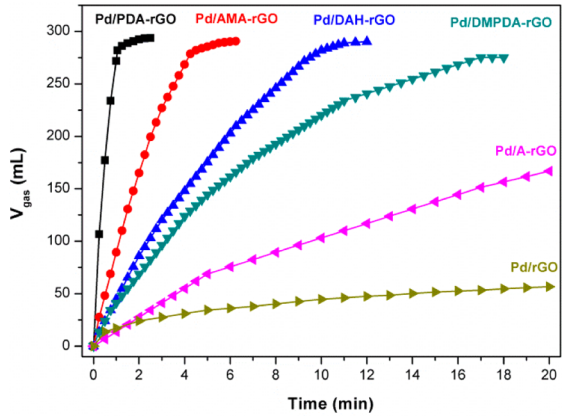

Figure 3. Volume of the generated gas (CO_2 + H_2) versus time for the dehydrogenation of FA over Pd/PDA-rGO, Pd/AMA-rGO, Pd/DAH-rGO, Pd/DMPDA-rGO, and Pd/rGO (n_{Pd}/n_{FA} = 0.015, FA/SF = 1:1, 323 K).

In summary, for the first time, the alkalization of GO with diamine in this work provides a powerful method to prepare ultrafine metal NPs and modifies the alkalinity of the support for optimizing the catalytic performance. By using the alkalized GO, well-dispersed ultrafine Pd NPs with a diameter below 1.5 nm can be readily obtained. Moreover, the diamine-alkalized rGO surface benefits the formation of unique amine-associated formate, the important intermediate for formic acid dehydrogenation. Owing to both of the effects from the high Pd dispersion and amine−formic acid interaction, the resultant Pd/PDA-rGO nanocatalysts exhibit significantly enhanced

DOI: 10.1021/acscatal.5b01411
ACS Catal. 2015, 5, 5141−5144

catalytic activity for dehydrogenation from FA under mild conditions, achieving the highest TOF value, with 100% H_2 selectivity, among those of heterogeneous catalysts. The present work provides an effective strategy to immobilize ultrafine metal NPs on GO, which have tremendous application prospect in various catalytic fields.

■ ASSOCIATED CONTENT

Supporting Information

The Supporting Information is available free of charge on the ACS Publications website at DOI: 10.1021/acscatal.5b01411.

Experimental details, additional material characterization, and catalytic performance (PDF)

■ AUTHOR INFORMATION

Corresponding Author

*E-mail: q.xu@aist.go.jp.

Author Contributions

§F.-Z.S. and Q.-L.Z. contributed equally.

Notes

The authors declare no competing financial interests.

■ ACKNOWLEDGMENTS

The authors are thankful to Dr. Yanying Zhao for Raman, Dr. Yasuyuki Matsumura for XPS, and Dr. Takeyuki Uchida for SEM and TEM measurements, and AIST and METI for financial support. F.-Z.S. thanks MEXT for a government scholarship.

■ REFERENCES

(1) (a) Farmer, J. A.; Campbell, C. T. *Science* **2010**, *329*, 933−936. (b) Li, P.-Z.; Aijaz, A.; Xu, Q. *Angew. Chem., Int. Ed.* **2012**, *51*, 6753−6756. (c) Aijaz, A.; Karkamkar, A.; Choi, Y. J.; Tsumori, N.; Rönnebro, E.; Autrey, T.; Shioyama, H.; Xu, Q. *J. Am. Chem. Soc.* **2012**, *134*, 13926−13929. (d) Yin, H.; Tang, H.; Wang, D.; Gao, Y.; Tang, Z. *ACS Nano* **2012**, *6*, 8288−8297. (e) Kuo, C.-H.; Tang, Y.; Chou, L.-Y.; Sneed, B. T.; Brodsky, C. N.; Zhao, Z.; Tsung, C.-K. *J. Am. Chem. Soc.* **2012**, *134*, 14345−14348. (f) Guo, Z.; Xiao, C.; Maligal-Ganesh, R. V.; Zhou, L.; Goh, T. W.; Li, X.; Tesfagaber, D.; Thiel, A.; Huang, W. *ACS Catal.* **2014**, *4*, 1340−1348.

(2) (a) Ping, Y.; Yan, J.-M.; Wang, Z.-L.; Wang, H.-L.; Jiang, Q. *J. Mater. Chem. A* **2013**, *1*, 12188−12191. (b) Tan, C.; Huang, X.; Zhang, H. *Mater. Today* **2013**, *16*, 29. (c) Liu, M.; Zhang, R.; Chen, W. *Chem. Rev.* **2014**, *114*, 5117−5160. (d) Wang, Z.-L.; Yan, J.-M.; Zhang, Y.-F.; Ping, Y.; Wang, H.-L.; Jiang, Q. *Nanoscale* **2014**, *6*, 3073−3077.

(3) (a) Guo, S.; Dong, S.; Wang, E. *ACS Nano* **2010**, *4*, 547−555. (b) Parvez, K.; Yang, S.; Hernandez, Y.; Winter, A.; Turchanin, A.; Feng, X.; Müllen, K. *ACS Nano* **2012**, *6*, 9541−9550. (c) Shin, S. I.; Go, A.; Kim, I. Y.; Lee, J. M.; Lee, Y.; Hwang, S.-J. *Energy Environ. Sci.* **2013**, *6*, 608−617. (d) Shang, L.; Bian, T.; Zhang, B.; Zhang, D.; Wu, L.-Z.; Tung, C.-H.; Yin, Y.; Zhang, T. *Angew. Chem., Int. Ed.* **2014**, *53*, 250−254. (e) Chen, Y.; Zhu, Q.-L.; Tsumori, N.; Xu, Q. *J. Am. Chem. Soc.* **2015**, *137*, 106−109.

(4) (a) Fellay, C.; Dyson, P. J.; Laurenczy, G. *Angew. Chem., Int. Ed.* **2008**, *47*, 3966−3968. (b) Ojeda, M.; Iglesia, E. *Angew. Chem., Int. Ed.* **2009**, *48*, 4800−4803. (c) Loges, B.; Boddien, A.; Gärtner, F.; Junge, H.; Beller, M. *Top. Catal.* **2010**, *53*, 902−914. (d) Boddien, A.; Mellmann, D.; Gärtner, F.; Jackstell, R.; Junge, H.; Dyson, P. J.; Laurenczy, G.; Ludwig, R.; Beller, M. *Science* **2011**, *333*, 1733−1736. (e) Hull, J. F.; Himeda, Y.; Wang, W.-H.; Hashiguchi, B.; Periana, R.; Szalda, D. J.; Muckerman, J. T.; Fujita, E. *Nat. Chem.* **2012**, *4*, 383−388. (f) Grasemann, M.; Laurenczy, G. *Energy Environ. Sci.* **2012**, *5*, 8171−8181. (g) Martis, M.; Mori, K.; Fujiwara, K.; Ahn, W.-S.; Yamashita, H. *J. Phys. Chem. C* **2013**, *117*, 22805−22810. (h) Moret, S.; Dyson, P. J.; Laurenczy, G. *Nat. Commun.* **2014**, *5*, 4017.

(5) (a) Loges, B.; Boddien, A.; Junge, H.; Beller, M. *Angew. Chem., Int. Ed.* **2008**, *47*, 3962−3965. (b) Himeda, Y. *Green Chem.* **2009**, *11*, 2018−2022. (c) Sponholz, P.; Mellmann, D.; Junge, H.; Beller, M. *ChemSusChem* **2013**, *6*, 1172−1176. (d) Gan, W.; Snelders, D. J. M.; Dyson, P. J.; Laurenczy, G. *ChemCatChem* **2013**, *5*, 1126−1132. (e) Thevenon, A.; Frost-Pennington, E.; Weijia, G.; Dalebrook, A. F.; Laurenczy, G. *ChemCatChem* **2014**, *6*, 3146−3152.

(6) (a) Gu, X.; Lu, Z.-H.; Jiang, H.-L.; Akita, T.; Xu, Q. *J. Am. Chem. Soc.* **2011**, *133*, 11822−11825. (b) Wang, Z.-L.; Yan, J.-M.; Ping, Y.; Wang, H.-L.; Zheng, W.-T.; Jiang, Q. *Angew. Chem., Int. Ed.* **2013**, *52*, 4406−4409. (c) Hu, C.; Pulleri, J. K.; Ting, S.-W.; Chan, K.-Y. *Int. J. Hydrogen Energy* **2014**, *39*, 381−390. (d) Yu, W.-Y.; Mullen, G. M.; Flaherty, D. W.; Mullins, C. B. *J. Am. Chem. Soc.* **2014**, *136*, 11070−11078. (e) Zhu, Q.-L.; Tsumori, N.; Xu, Q. *Chem. Sci.* **2014**, *5*, 195−199. (f) Zhu, Q.-L.; Xu, Q. *Energy Environ. Sci.* **2015**, *8*, 478−512.

(7) (a) Chen, R.; Zhao, T.; Lu, J.; Wu, F.; Li, L.; Chen, J.; Tan, G.; Ye, Y.; Amine, K. *Nano Lett.* **2013**, *13*, 4642−4649. (b) Hu, H.; Zhao, Z.; Wan, W.; Gogotsi, Y.; Qiu, J. *Adv. Mater.* **2013**, *25*, 2219−2223. (c) Wang, Z.; Dong, Y.; Li, H.; Zhao, Z.; Wu, H. B.; Hao, C.; Liu, S.; Qiu, J.; Lou, X. W. *Nat. Commun.* **2014**, *5*, 5002.

(8) (a) Kudin, K. N.; Ozbas, B.; Schniepp, H. C.; Prud'homme, R. K.; Aksay, I. A.; Car, R. *Nano Lett.* **2008**, *8*, 36−41. (b) Malard, L. M.; Pimenta, M. A.; Dresselhaus, G.; Dresselhaus, M. S. *Phys. Rep.* **2009**, *473*, 51−87. (c) Lee, C.-W.; Yoon, S.-B.; Kim, H.-K.; Youn, H.-C.; Han, J.; Roh, K. C.; Kim, K.-B. *J. Mater. Chem. A* **2015**, *3*, 2314−2322.

(9) Tiwari, J. N.; Nath, K.; Kumar, S.; Tiwari, R. N.; Kemp, K. C.; Le, N. H.; Youn, D. H.; Lee, J. S.; Kim, K. S. *Nat. Commun.* **2013**, *4*, 2221.

(10) (a) Yadav, M.; Akita, T.; Tsumori, N.; Xu, Q. *J. Mater. Chem.* **2012**, *22*, 12582−12586. (b) Bi, Q.-Y.; Du, X.-L.; Liu, Y.-M.; Cao, Y.; He, H.-Y.; Fan, K.-N. *J. Am. Chem. Soc.* **2012**, *134*, 8926−8933. (c) Mori, K.; Dojo, M.; Yamashita, H. *ACS Catal.* **2013**, *3*, 1114−1119.

DOI: 10.1021/acscatal.5b01411
ACS Catal. 2015, 5, 5141−5144